Neutrino production in the cores of active galaxies

A.M. Carulli[1,2], M.M. Reynoso[1,2] & L.P. Duvidovich[1,2]

[1] *Instituto de Investigaciones Físicas de Mar del Plata, CONICET–UNMdP, Argentina*
[2] *Departamento de Física, Facultad de Ciencias Exactas y Naturales, UNMdP, Argentina*

Received: 09 February 2024 / Accepted: 20 May 2024

Resumen / Los núcleos de galaxias activas, como NGC 1068, pueden ser fuentes de neutrinos de alta energía y son opacos a los rayos gamma de alta energía. Los parámetros que caracterizan las regiones de aceleración que conducen a la producción de neutrinos no están claros. En este trabajo presentamos un modelo de producción de neutrinos en chorros que emergen de agujeros negros de masa estelar que están embebidos en el disco de acreción de núcleos galácticos activos. Los resultados obtenidos son consistentes con el flujo electromagnético observado en bandas de diferentes longitudes de ondas. Analizamos las consecuencias de la variación de parámetros como el campo magnético de la región de producción de neutrinos, su tamaño y la influencia del entorno circundante.

Abstract / The cores of active galaxies, such as NGC 1068, can be sources of high-energy neutrinos, and are opaque to high-energy gamma rays. The parameters that characterize the acceleration regions leading to neutrino production are not clear. In this work we present a model of neutrino production in jets emerging from stellar-mass black holes that are embedded in the accretion disk of active galactic nuclei. The results obtained are consistent with the electromagnetic flux observed in different wavebands. We analyze the consequences of varying parameters such as the magnetic field of the neutrino production region, its size, and the influence of the surrounding environment.

Keywords / neutrinos — astroparticle physics — galaxies: active

1. Introduction

The IceCube collaboration reported neutrino observations from NGC 1068 (Aartsen et al. 2020), a Seyfert galaxy located at 12.7 Mpc from Earth. The mechanism that explains the origin of these neutrinos is unclear. This source has been observed in different wavelenghts. The inner regions were observed by *ALMA* in the near-infrared to radio (García-Burillo et al. 2019). There are also radio observations of the outer regions ($\sim$ 100 pc) (Sajina et al. 2011). Furthermore, gamma rays can be observed up to energies of 100 GeV (Ajello et al. 2017; Acciari et al. 2019; Abdollahi et al. 2020). Many efforts have been made to understand the nonthermal emission from radio-quiet active galactic nuclei (AGN), such as hot coronae models (Murase et al. 2020; Eichmann et al. 2022), hot accretion flows (Gutiérrez et al. 2021) and accretion shocks (Inoue et al. 2020), among others. The problem arises from the connection between the production of neutrinos and gamma rays, since the processes that lead to the production of neutrinos must not have an associated gamma ray counterpart that violates the available observational data.

In this work, we show preliminary results of a jet model emerging from stellar-mass black holes (sBH) embedded in AGN accretion disks (see Fig.1). We apply this model following the idea proposed by Tagawa et al. (2023), which consists on taking sBHs as sources of the emission detected in AGNs, and here we use steady-state transport equations to describe the populations electrons and protons accelerated by inner shocks in the jets of sBHs. This approach allows for a neutrino production scenario and strong suppression of the associated gamma rays.

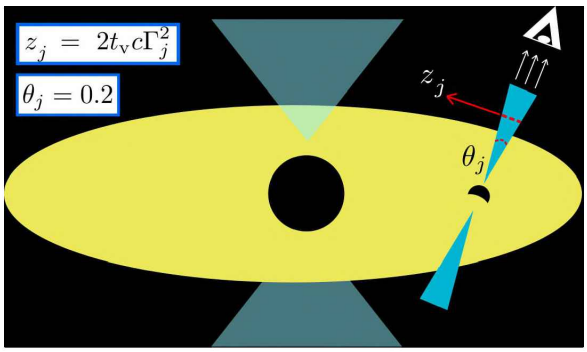

Fig. 1. Schematic view of the sBH prototype adopted in our model. We show the point of injection z_j and the opening angle of the jet θ_j.

2. Model

In order to model the emission produced in a jet emerging from a sBH, we consider an homogeneous region within it. The characteristic size of the emission region is $\Delta z_j \approx z_j\,\theta_j$, where z_j is the distance at which we place the injection zone and θ_j is the opening angle of the jet.

The volume of the region is taken as in Denton & Tamborra (2018):

$$\Delta V = 4\,\pi\,(1-\cos\theta_j)\,z_j^2\,c\,t_v\,\Gamma_j, \quad (1)$$

✉ *Contact* / amcarulli@mdp.edu.ar

Table 1. Input and derived parameters.

Parameters	Description	s1	s2	s3
$L_{\rm j}$ (erg s^{-1})	jet luminosity	2×10^{42}	2×10^{42}	2×10^{42}
Γ	Lorentz factor	8	4	4
η	acceleration efficiency	0.001	0.01	0.01
$q_{\rm rel}$	ratio $(L_{\rm e}+L_{\rm p})/L_{\rm k}$	0.07	0.1	0.2
a	ratio $L_{\rm p}/L_{\rm e}$	10	1	3
$\epsilon_{\rm B}$	magnetic field energy fraction	0.1	0.05	0.3
Δz (cm)	emission size	7.8×10^{8}	1.9×10^{8}	1.9×10^{8}
B (G)	magnetic field	1.6×10^{5}	2.5×10^{6}	1.9×10^{7}
$n_{\rm p,cold}$ (cm^{-3})	density of cold protons	1.9×10^{14}	1.2×10^{16}	1.2×10^{16}
α	injection index	2.6	2.2	2.2

where the variability timescale of the jet is $t_{\rm v}=10^{-3}$ s.

The luminosity of the jet is taken as $L_{\rm j}=\eta_j\,\dot{m}\,c^2\approx 2\times10^{42}$ erg s^{-1}, which corresponds to a super-Eddington accretion rate of $\dot{m}=3\times10^{-4}\ M_\odot\,{\rm yr}^{-1}\,(\eta_{\rm j}/0.1)^{-1}$, where $\eta_j=0.1$ represents the efficiency with which the jet engine converts energy into kinetic energy (Tagawa et al., 2023). Assuming that each sBH accretes for $\sim$ 4 Myr per AGN phase and the accretion rate is constant, the mass of an sBH increases to $m\sim10^3\ M_\odot$. The fraction of the jet luminosity that is transfered to electrons and protons is $L_{\rm p}+L_{\rm e}=q_{\rm rel}\,L_{\rm j}$, where the relation between the luminosity of protons and electrons depends on the parameter a as $L_{\rm p}=a\,L_{\rm e}$.

The cold proton density in the jet can be obtained as (Tagawa et al. 2023):

$$n_{\rm p}=\left(\frac{2L_j}{\theta_{\rm j}^2}\right)\frac{1}{4\,\pi\,\Gamma_{\rm j}^2\,z_{\rm j}^2\,m_{\rm p}\,c^3}, \tag{2}$$

where the first factor in the right hand side of the equation is the isotropic luminosity (Denton & Tamborra, 2018).

On the other hand, the magnetic field is obtained as (Tagawa et al. 2023):

$$B_{\rm j}=\sqrt{8\,\pi\,\epsilon_{\rm B}\,e_{\rm j}}, \tag{3}$$

where $e_{\rm j}=2.7\,n_{\rm p}\,m_{\rm p}\,c^2$ is the internal energy density of the shocked jet, and $\epsilon_{\rm B}$ is the fraction of postshock energy carried by protons and electrons.

In order to calculate the distribution of primary protons and electrons, we solve the steady-state transport equation

$$\frac{{\rm d}\,[b_i\,N_i(E_i)]}{{\rm d}E}+\frac{N_i(E_i)}{T_{\rm esc}}=Q_i(E_i), \tag{4}$$

where $b_i\equiv dE_i/dt=-E_i\,t_{\rm cool}^{-1}$ denote the energy losses of the particles and the injection of primary particles can be expressed like

$$Q_i(E_i)=K_i\,E_i^{-\alpha}\,{\rm e}^{(-E_i/E_{{\rm max},i})}. \tag{5}$$

The constant K_i is fixed by normalization on the total power injected in electrons and protons

$$L_i=4\,\pi\,\Delta V\int_{E_{i,\rm min}}^{\infty}{\rm d}E_i\,E\,Q_i(E_i). \tag{6}$$

Notice that, rather than assuming the primary particle distributions follow a power law in energy, as in Tagawa et al. (2023), we consider an injection that follows a power law in energy, as described in Eq.(4), and then solve Eq.(5).

In order to obtain the maximum energy $E_{{\rm max},i}$, we balance the cooling rates due to radiative processes plus the escape rate with the particle acceleration rate.

Neutrinos are produced when protons collide with cold protons in the jet or when they interact with photons produced via synchrotron of electrons. These interactions produce charged pions that produce neutrinos and muons. We follow Kelner et al. (2006) and Hümmer et al. (2010) to calculate pions produced from proton-proton (pp) and proton-gamma ($p\gamma$) interactions respectively. Muons also decay to neutrinos. We follow Lipari et al. (2007) to calculate the neutrino fluxes. On the other hand, neutral pions decay to produce gamma rays. We follow Kelner et al. (2006) and expressions therein to obtain the gamma ray fluxes by pp interactions, and refer to Kelner & Aharonian (2008) to calculate those originated by $p\gamma$ interactions. We consider internal absorption effects that are due to electron synchrotron and IC radiation, and we account for it by multiplying the emission by a factor $(1-\exp(-\tau_{\gamma\gamma}))/\tau_{\gamma\gamma}$, where $\tau_{\gamma\gamma}$ is the optical depth of the process.

3. Results and discussion

We consider three sets of parameters, named s1, s2 and s3, for which we vary the jet luminosity, the lorentz factor, the magnetic field, the cold proton target, the size of the zone and the injection index, as shown in Table 1.

In Fig. 2 we show the cooling rates of primary particles as a function of the energy for the models s1, s2 and s3. In the case of electrons, due to the high magnetic field, the synchrotron cooling dominates for all the sets of parameters, but IC is significant as well. In the case of protons, proton-proton (pp) interactions are important for lower energies, whereas synchrotron and pγ dominates the cooling rates for sets s2 and s3 at higher energies, and pγ dominates in the case of s1. Bohm diffusion was taken for the three sets. In Fig. 3 we show the resulting proton and electron distributions for the models s1, s2 and s3.

In Fig. 4 we show the resulting electromagnatic emission for the three parameter sets. The emission is

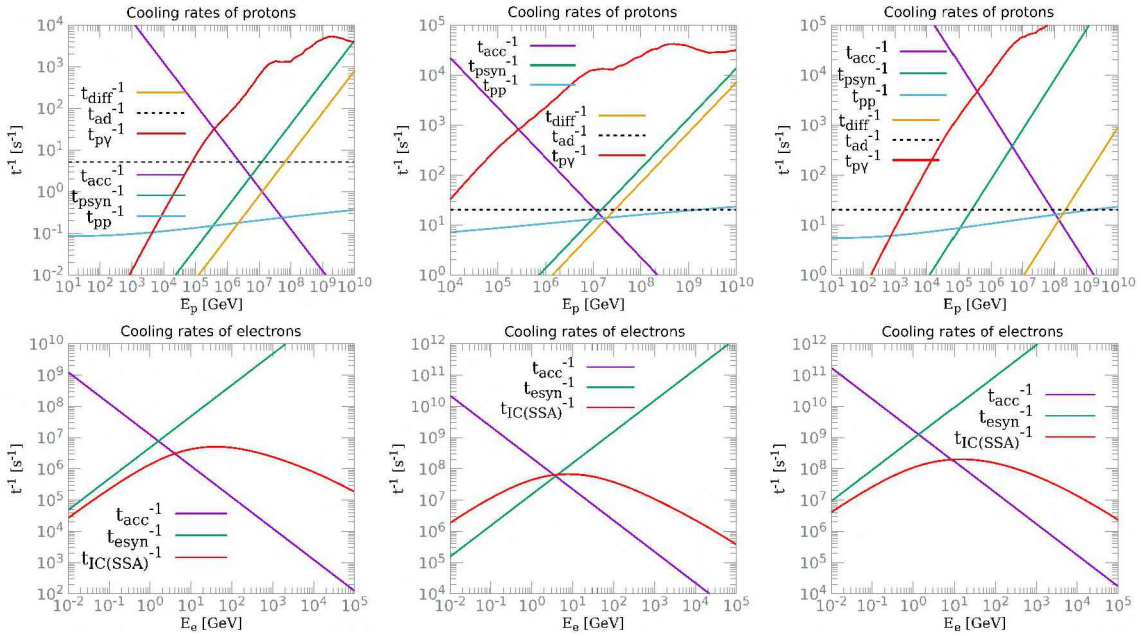

Fig. 2. *Top panels:* Proton cooling rates for the models s1 (*left panel*), s2 (*middle panel*) and s3 (*right panel*). *Bottom panels*: same as above but for electrons.

dominated by the synchrotron of electrons and IC for the three cases, due to the intensity of the magnetic field. It can be seen that for all the cases, the gamma-ray flux suffers a strong suppresion at energies greater than ~ 1 GeV for model s1, and ~ 0.1 GeV for models s2 and s3.

In Fig. 5 we show the resulting neutrinos fluxes and compare it with the uncertainties on the spectrum measured by Aartsen et al. (2020). The contribution to the neutrino flux is dominated by $p\gamma$ interactions for the high energy regime in the three models, whereas pp interactions dominates the emission for energies $\lesssim 10^4$GeV for s1 and $\lesssim 10^3$GeV for s2 and s3. These contributions can explain the data of the neutrino flux detected by IceCube for NGC 1068 (Aartsen et al. 2020), when we consider the set of parameters s3. On the other hand, s2 barely reaches the neutrino flux detected for 10^4GeV, while the set s1 does not produce enough neutrinos to reach the data.

4. Conclusion

We develop a model that allows to obtain a single object neutrino and photon flux produced by jets embedded in AGNs. In particular, we model neutrinos and gamma-rays emissivities for NGC 1068. The neutrino flux originated due to $p\gamma$ interactions could reach the observed flux reported by Aartsen et al. (2020), when we consider the set of parameters s3. Future neutrino telescopes such as the next IceCube generation 2 (*IC Gen2*) (van Santen, 2017) and *KM3NeT* (Aiello et al., 2019) will provide further constrains to the model parameters. On the other hand, the main contribution to the electromagnetic flux is due to synchrotron of electrons and IC. In the gamma-ray band, $p\gamma$ an pp could be significant if internal absortion is not considered. The internal absorption is due to these electrons and supress all the flux for energies greater than ~ 1 GeV for model s1, and ~ 0.1 GeV for models s2 and s3.

Acknowledgements: We thank ANPCyT and Universidad Nacional de Mar del Plata for their financial support through grants PICT 2021-GRF-T1-00725 and EXA1214/24, respectively.

References

Aartsen M.G., et al., 2020, Phys. Rev. Lett., 124, 051103
Abdollahi S., et al., 2020, ApJS, 247, 33
Acciari V.A., et al., 2019, The Astrophysical Journal, 883, 135
Aiello S., et al., 2019, Astroparticle Physics, 111, 100
Ajello M., et al., 2017, ApJS, 232, 18
Denton P.B., Tamborra I., 2018, Astrophys. J., 855, 37
Eichmann B., et al., 2022, The Astrophysical Journal, 939, 43
García-Burillo S., et al., 2019, A&A, 632, A61
Gutiérrez E.M., Vieyro F.L., Romero G.E., 2021, A&A, 649, A87
Hümmer S., et al., 2010, The Astrophysical Journal, 721, 630
Inoue Y., Khangulyan D., Doi A., 2020, ApJL, 891, L33
Kelner S.R., Aharonian F.A., 2008, Phys. Rev. D, 78, 034013
Kelner S.R., Aharonian F.A., Bugayov V.V., 2006, Phys. Rev. D, 74, 034018
Lipari P., Lusignoli M., Meloni D., 2007, Phys. Rev. D, 75, 123005
Murase K., Kimura S.S., Mészáros P., 2020, PhRvL, 125, 011101
Sajina A., et al., 2011, ApJ, 732, 45
Tagawa H., Kimura S.S., Haiman Z., 2023
van Santen J., 2017, PoS, ICRC2017, 991

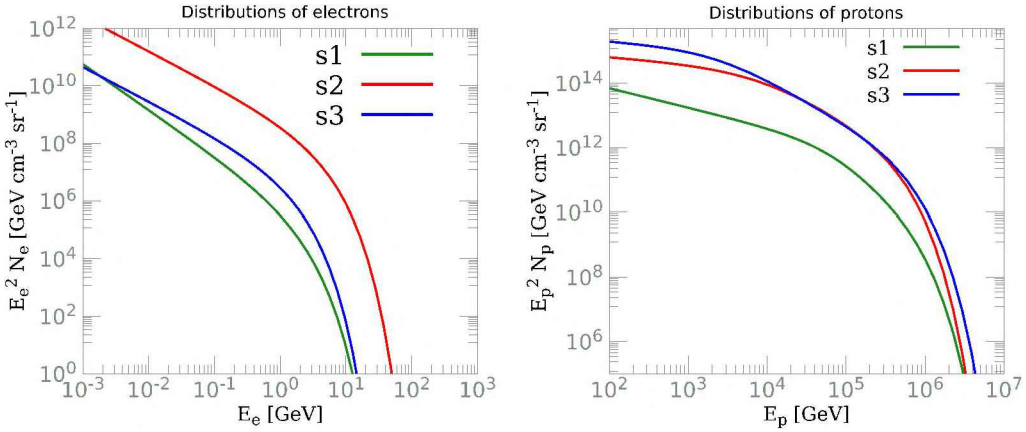

Fig. 3. *Left panel:* Electron distributions as a function of the energy, adopting the parameters in table 1 for the models s1, s2 and s3. *Right panel:* same as *left panel* but for protons

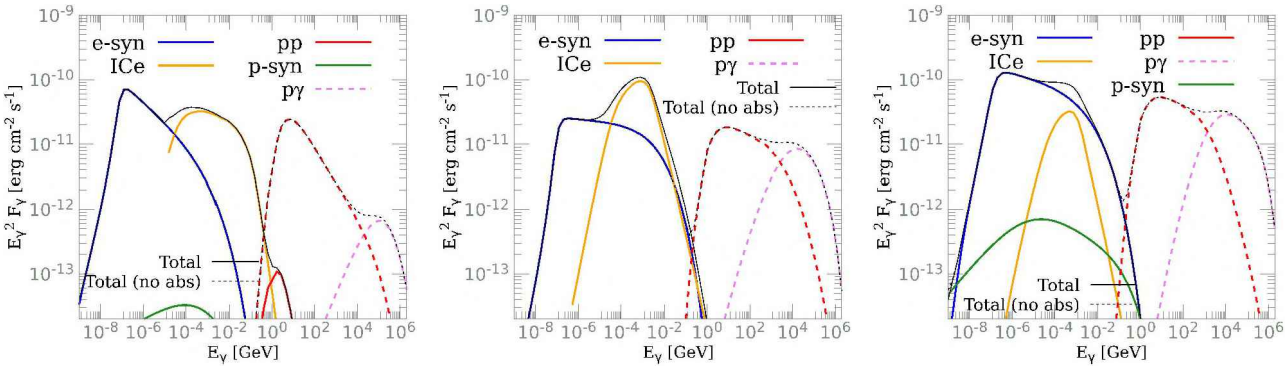

Fig. 4. *Left panel:* Photon fluxes as a function of the energy for the model s1. Curves with different colors correspond with different processes as indicated in the legend, as well as the total emission. Dashed lines correspond to the emission with no absorption. *Middle panel:* same as *left panel* but for the model s2. *Right panel:* same as *left panel* but for the model s3.

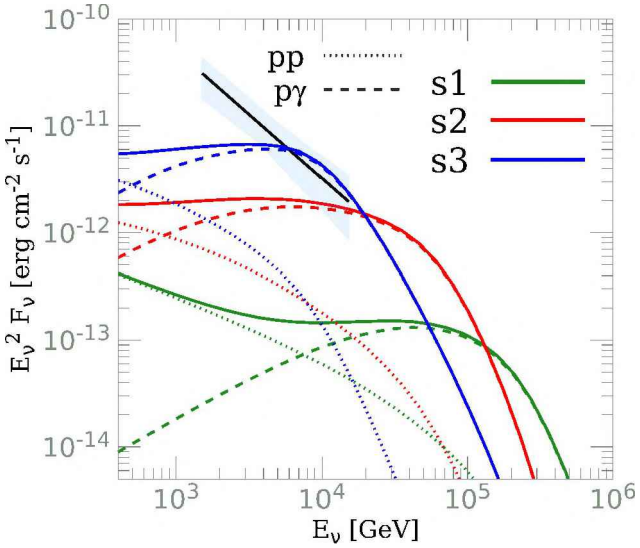

Fig. 5. Neutrino fluxes as a function of the energy for the models s1, s2 and s3. The blue shaded region represents 1σ uncertainty on the spectrum measured by Aartsen et al. (2020).